Available online at www.sciencedirect.com
ScienceDirect
Journal of Sound and Vibration 322 (2009) 612–628
JOURNAL OF SOUND AND VIBRATION
www.elsevier.com/locate/jsvi

Instabilities in the main parametric resonance area of a mechanical system with a pendulum

Jerzy Warminski*, Krzysztof Kecik

Department of Applied Mechanics, Lublin University of Technology, Nadbystrzycka 36, 20-618 Lublin, Poland

Accepted 23 June 2008
The peer review of this article was organised by the Guest Editor
Available online 15 August 2008

Abstract

Vibrations of an autoparametric system, composed of a nonlinear mechanical oscillator with an attached damped pendulum, around the principal resonance region, are investigated in this paper. Approximate analytical solutions of the model are determined on the basis of the Harmonic Balance Method (HBM). Correctness of the analytical results is verified by numerical simulations and experimental tests performed on an especially prepared experimental rig. The influence of all essential parameters such as damping, excitation amplitude and frequency, nonlinear stiffness of the spring, on the localisation of the instability region and the system dynamics is presented in the work. Regions of regular system oscillations, chaotic motions, and full rotation of the pendulum are confirmed experimentally.

1. Introduction

An autoparametric system differs from a parametric system because vibrations are caused by internal coupling involving at least two modes. From the mathematical point of view, the excitation comes from nonlinear coupling terms present in the equations of motion [1]. This kind of model can lead to an energy transfer between different vibration modes, as well as to resonances, possible only in this specific problem.

Autoparametric vibrations of an excited oscillator with an attached pendulum have been analysed in many papers in different aspects. This two degree-of-freedom system represents an interesting physical dynamical structure, which finds important practical engineering applications. Special dampers mounted in buildings and working against earthquakes, or against river vortices [2] (Fig. 1a and b), pendulums mounted on high chimneys [3], all can be mentioned as examples. Tondl et al. [4] cite several other applications of such systems.

The phenomenon of vibrations absorption of the mass-spring oscillator, defined as the main system, can be achieved due to proper pendulum swinging. However, for some parameters the situation may worsen and pendulum vibrations may increase dramatically, then the protection of the structure (modelled as a mass-spring oscillator) is lost [5]. Despite the fact that the main system is periodically excited, its response can be periodic, quasi-periodic, or even chaotic [4], for different system parameter combinations. Paper [6] presents

*Corresponding author. Tel.: +48 81 538 41 98; fax: +48 81 524 10 04.
E-mail addresses: j.warminski@pollub.pl (J. Warminski), k.kecik@pollub.pl (K. Kecik).

0022-460X/$ - see front matter © 2008 Elsevier Ltd. All rights reserved.
doi:10.1016/j.jsv.2008.06.042

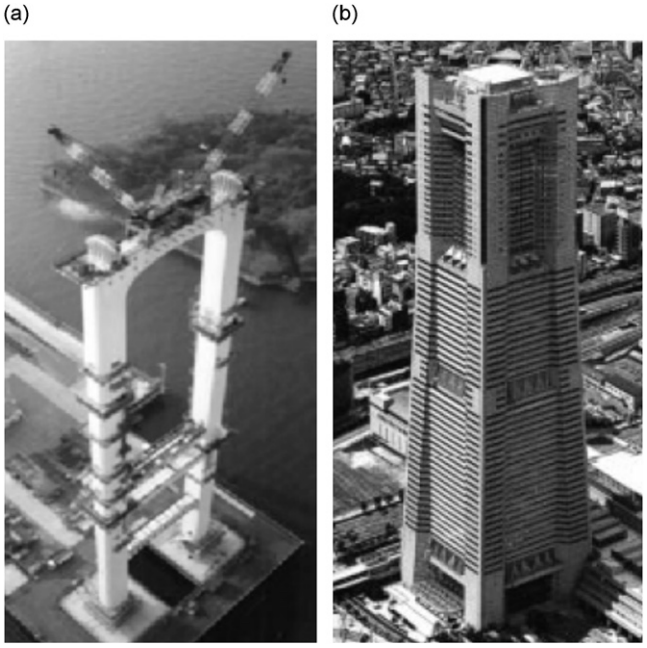

Fig. 1. A pendulum mounted on a bridge tower (a) and a pendulum mounted in Yokohama Landmark Tower (b) [2].

the method of averaging to study forced, weakly nonlinear oscillations of a two degree-of-freedom autoparametric vibration absorber around the resonant region. Hatwal et al. [7–9] show periodically modulated motions and chaos of an autoparametric system with a pendulum. The response of the resonantly excited autoparametric system, near the internal resonance, is shown in Ref. [10]. It has been found that the system motions undergo a pitchfork bifurcation to motion in which a pendulum executes nonzero response and then the oscillator vibrates with a very low amplitude.

The purpose of this paper is to study new dynamical phenomena of the coupled oscillator–pendulum system for realistic data, and then to check possible instability region occurrence. The dynamics inside this region and the influence of a nonlinear supporting spring as a possible new element which may eliminate or shift unwanted instability, are analysed numerically, and in detail. First, various solutions for the lower position of the pendulum and the influence of individual parameters on system dynamics, as well as transition to two different types of chaotic responses are demonstrated. Then, experimental tests which confirm chosen theoretical results are presented.

2. Model of the vibrating system and equations of motions

The considered mechanical model, presented in Fig. 2, consists of two main subsystems: (I) a nonlinear oscillator composed of a mass m_1 and a nonlinear spring and, (II) a pendulum made of two masses m_p and m_2. The pendulum is attached at a pivot to the mass m_1. The oscillator is forced by a classical linear spring due to motion of the base (kinematical excitation). The stiffness of the oscillator's spring is assumed to be nonlinear Duffing type function:

$$F_s = kx + k_1 x^3 \tag{1}$$

The motion of the model is described by two generalised coordinates namely the displacement of the oscillator in the vertical direction x, and the angle of the pendulum rotation φ. Viscous damping of the pendulum and the oscillator is expressed by the c_φ and c coefficients, respectively. The length of the pendulum is denoted by l.

The differential equations of motions are derived by application of Lagrange's equations of the second kind:

$$(m_1 + m_2 + m_p)\ddot{x} + c\dot{x} + (k + k_2)x + k_1 x^3 + \left(m_2 + \tfrac{1}{2}m_p\right) l(\ddot{\varphi} \sin \varphi + \dot{\varphi}^2 \cos \varphi) = k_2 Q \cos \omega t \tag{2}$$

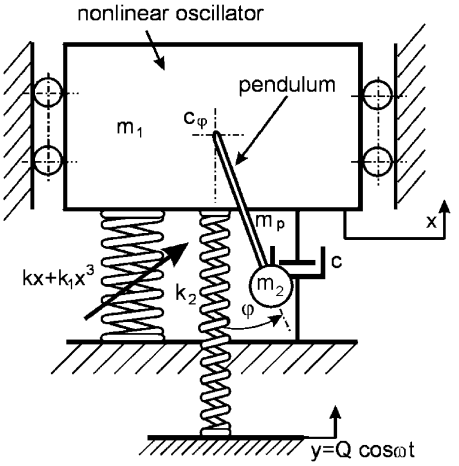

Fig. 2. A physical model of the autoparametric system.

$$\left(m_2+\tfrac{1}{3}m_p\right)l^2\ddot{\varphi}+c_\varphi\dot{\varphi}+\left(m_2+\tfrac{1}{2}m_p\right)l(\ddot{x}+g)\,\sin\,\varphi=0 \tag{3}$$

Eqs. (2) and (3) are typical for this type of autoparametric two degree-of-freedom system [11]. The nonlinear term of the supporting spring is a new element which appears in the model. Introducing dimensionless time $\tau=\omega_0 t$, where $\omega_0=\sqrt{(k+k_2)/(m_1+m_2+m_p)}$ is the natural frequency of the oscillator, and then the dimensionless coordinates $X=x/x_{st}$ and $\varphi\equiv\varphi$, where $x_{st}=(m_1+m_2+m_p)g/(k+k_2)$ is the static displacement of the linear oscillator, we express the equations of motion in the dimensionless form:

$$\ddot{X}+\alpha_1\dot{X}+X+\gamma X^3+\mu\lambda(\ddot{\varphi}\,\sin\,\varphi+\dot{\varphi}^2\,\cos\,\varphi)=q\,\cos\,\vartheta\tau \tag{4}$$

$$\ddot{\varphi}+\alpha_2\dot{\varphi}+\lambda(\ddot{X}+1)\,\sin\,\varphi=0 \tag{5}$$

The natural frequency of the linear oscillator is normalised to unity in Eq. (4). Dimensionless parameters take the following definitions:

$$\begin{aligned}&\alpha_1=\frac{c}{(m_1+m_2+m_p)\omega_0},\quad \alpha_2=\frac{c_\varphi}{(m_2+(1/3)m_p)l^2\omega_0},\quad \vartheta=\frac{\omega}{\omega_0}\\ &\mu=\frac{(m_2+(1/3)m_p)l^2}{(m_1+m_2+m_p)x_{st}^2},\quad \lambda=\frac{(m_2+(1/2)m_p)x_{st}}{(m_2+(1/3)m_p)l},\quad q=\frac{k_2Q}{(k+k_2)x_{st}},\quad \gamma=\frac{k_1}{k+k_2}x_{st}^2.\end{aligned} \tag{6}$$

Autoparametric excitation in Eq. (4) is caused by the coupling terms, i.e. the second derivative and the square of the first derivative, of the pendulum coordinate φ.

3. Approximate analytical solutions

Because the equations of motions (4) and (5) include nonlinear terms it is difficult to find their strictly correct solutions. Therefore, in the neighbourhood of principal parametric resonance approximate solutions are sought. Around this area the mass m_1 vibrates with frequency ϑ, which is equal to the excitation frequency, while the pendulum oscillates with frequency $\vartheta/2$. On the basis of this assumption we seek solutions in the form of

$$\begin{aligned}x(\tau)&=A(\tau)\,\cos(\vartheta\tau+\phi_1(\tau))\\ \varphi(\tau)&=B(\tau)\,\cos\left(\frac{\vartheta}{2}\tau+\phi_2(\tau)\right)\end{aligned} \tag{7}$$

Taking into account small oscillations of the pendulum around the equilibrium point $\varphi \approx 0$, the nonlinear terms $\sin\varphi$ and $\cos\varphi$ are expanded by Taylor's series

$$\sin\varphi = \varphi - \frac{\varphi^3}{6}, \quad \cos\varphi = 1 - \frac{\varphi^2}{2} \tag{8}$$

Amplitudes $A(\tau)$, $B(\tau)$ and phases $\phi_1(\tau)$, $\phi_2(\tau)$ describe the oscillator and pendulum motions, respectively. For better clarity, the $A(\tau)\equiv A$, $B(\tau)\equiv B$, $\phi_1(\tau)\equiv\phi_1$, $\phi_2(\tau)\equiv\phi_2$ notations are used. Introducing Eqs. (7) and (8) into Eqs. (4) and (5), and then balancing the coefficients of the corresponding *sine* and *cosine* terms, we get a set of first-order approximate differential equations:

$$\begin{aligned}
&\alpha_1\dot{A} + \dot{B}\sin(\phi_1 - 2\phi_2)\left(2\frac{\vartheta}{2}\mu\lambda B - \frac{1}{3}\frac{\vartheta}{2}\mu\lambda B^3\right) - 2\vartheta A\dot{\phi}_1 - 2\frac{\vartheta}{2}\mu\lambda B^2\dot{\phi}_2\cos(\phi_1 - 2\phi_2)\\
&\quad + \frac{1}{6}\left(\frac{\vartheta}{2}\right)\mu\lambda B^4\dot{\phi}_2\cos(\phi_1 - 2\phi_2) + A(1-\vartheta^2) + \frac{3}{4}\gamma A^3 - \left(\frac{\vartheta}{2}\right)^2\mu\lambda B^2\cos(\phi_1 - 2\phi_2)\\
&\quad + \frac{1}{12}\left(\frac{\vartheta}{2}\right)^2\mu\lambda B^4\cos(\phi_1 - 2\phi_2) - q\cos(\phi_1) = 0
\end{aligned} \tag{9}$$

$$\begin{aligned}
&-2\vartheta\dot{A} + \dot{B}\cos(\phi_1 - 2\phi_2)\left(-2\frac{\vartheta}{2}\mu\lambda B + \frac{1}{3}\frac{\vartheta}{2}\mu\lambda B^3\right) - \alpha_1 A\dot{\phi}_1 - 2\frac{\vartheta}{2}\mu\lambda B^2\dot{\phi}_2\sin(\phi_1 - 2\phi_2)\\
&\quad + \frac{1}{6}\left(\frac{\vartheta}{2}\right)\mu\lambda B^4\dot{\phi}_2\sin(\phi_1 - 2\phi_2) - \alpha_1\vartheta A - \left(\frac{\vartheta}{2}\right)^2\mu\lambda B^2\sin(\phi_1 - 2\phi_2) + \frac{1}{12}\left(\frac{\vartheta}{2}\right)^2\\
&\quad \times \mu\lambda B^4\sin(\phi_1 - 2\phi_2) - q\sin(\phi_1) = 0
\end{aligned} \tag{10}$$

$$\begin{aligned}
&\alpha_2\dot{B} - \dot{\phi}_1\cos(\phi_1 - 2\phi_2)\left(\vartheta\lambda AB - \frac{1}{8}\lambda\vartheta AB^3\right) - 2\frac{\vartheta}{2}B\dot{\phi}_2 - B\left(\left(\frac{\vartheta}{2}\right)^2 - \lambda + \frac{1}{8}\lambda B^2\right)\\
&\quad - \cos(\phi_1 - 2\phi_2)\left(\frac{1}{2}\lambda\vartheta^2 AB - \frac{1}{16}\lambda\vartheta^2 AB^3\right) = 0
\end{aligned} \tag{11}$$

$$\begin{aligned}
&-2\frac{\vartheta}{2}\dot{B} + \dot{\phi}_1\sin(\phi_1 - 2\phi_2)\left(\lambda\vartheta AB - \frac{1}{8}\lambda\vartheta AB^3\right) - \alpha_2 B\dot{\phi}_2 - \alpha_2 B\left(\frac{\vartheta}{2}\right)\\
&\quad + \sin(\phi_1 - 2\phi_2)\left(\frac{1}{2}\lambda\vartheta^2 AB - \frac{1}{16}\lambda\vartheta^2 AB^3\right) = 0
\end{aligned} \tag{12}$$

Assuming that amplitudes and phases are slow functions of time, the derivatives of the second order, and terms having derivatives of a power higher then one, are neglected in the equations above. Furthermore, according to paper [12], in which the so-called Improved Harmonic Balance Method (HBM) is proposed, for small oscillations of the pendulum we may assume

$$\frac{B^4}{48} \approx 0, \quad \frac{B^3}{16} \approx 0 \tag{13}$$

For a steady state, amplitudes and phases are constant, thus the first-order derivatives are equal to zero

$$\dot{A} = 0, \quad \dot{B} = 0, \quad \dot{\phi}_1 = 0, \quad \dot{\phi}_2 = 0 \tag{14}$$

Introducing Eq. (14) into Eqs. (9)–(12), and taking into account the simplifications mentioned above we obtain the following equation:

$$(1-\vartheta^2)A + \frac{3}{4}\gamma A^3 - \mu\lambda\left(\frac{\vartheta}{2}\right)^2 B^2\cos(2\phi_2 - \phi_1) = q\cos\phi_1 \tag{15}$$

$$-\vartheta\alpha_1 A + \mu\lambda\left(\frac{\vartheta}{2}\right)^2 B^2 \sin(2\phi_2 - \phi_1) = q \sin\phi_1 \tag{16}$$

$$\left(\frac{\vartheta}{2}\right)^2 - \lambda + \frac{\lambda}{8}B^2 + A\frac{\lambda\vartheta^2}{2}\cos(2\phi_2 - \phi_1) = 0 \tag{17}$$

$$\alpha_2\left(\frac{\vartheta}{2}\right) + A\frac{\lambda\vartheta^2}{2}\sin(2\phi_2 - \phi_1) = 0 \tag{18}$$

The solutions of the nonlinear algebraic Eqs. (15)–(18) represent amplitudes and phases of the model response in the steady state. It has not been possible to obtain solutions of these equations in analytical form. However, if the nonlinearity of the spring is neglected, $\gamma = 0$, we can determine A^2 from Eqs. (15) and (16) and A^2 from Eqs. (17) and (18)

$$A^2 = \frac{B^4}{16\vartheta^4} + \frac{B^2(4\lambda\vartheta^2 - 16\lambda^2)}{16\lambda^2\vartheta^4} + \frac{64\lambda^2 - 32\vartheta^2\lambda + 4\vartheta^4 + 16\vartheta^2\alpha_2^2}{16\lambda^2\vartheta^4} \tag{19}$$

$$A^2 = \frac{\mu\lambda B^4(2\vartheta^2 - 2 - \mu\lambda\vartheta^4)}{16(1 + (-2 + \alpha_1^2)\vartheta^2 + \vartheta^4)} + \frac{4\mu\lambda B^2(3 - 3\vartheta^2 - 2\alpha_1\alpha_2)}{16(1 + (-2 + \alpha_1^2)\vartheta^2 + \vartheta^4)} + \frac{q^2}{1 + \vartheta^2(-2 + \alpha_1^2) + \vartheta^4} \tag{20}$$

Then, equating Eqs. (19) and (20), and making some algebraic manipulations we find the following equations

$$B^4\left(\frac{-\lambda^2\mu^2\vartheta^4 + 2\lambda\mu(-1 + \vartheta^2)}{16(1 + (-2 + \alpha_1^2)\vartheta^2 + \vartheta^4)} - \frac{1}{16\vartheta^4}\right) + B^2\left(\frac{-16\lambda\mu(-1 + \vartheta^2) + 4\mu\vartheta^2(-1 - 2\alpha_1\alpha_2 + \vartheta^2)}{16(1 + (-2 + \alpha_1^2)\vartheta^2 + \vartheta^4)} - \frac{-16\lambda^2 + 4\lambda\vartheta^2}{16\lambda^2\vartheta^4}\right)$$
$$+ \frac{q^2}{1 + \vartheta^2(-2 + \alpha_1^2) + \vartheta^4} - \frac{64\lambda^2 - 32\lambda\vartheta^2 + 4(4\alpha_2^2\vartheta^2 + \vartheta^4)}{16\lambda^2\vartheta^4} = 0 \tag{21}$$

$$\tan\phi_1 = \frac{4\vartheta(4A^2\alpha_1 + B^2\alpha_2\mu)}{16A^2(\vartheta^2 - 1) - B^2\mu((B^2 - 8)\lambda + 2\vartheta^2)}$$
$$\tan(2\phi_2 - \phi_1) = \frac{\alpha_2(\vartheta/2)}{(\vartheta/2)^2 - \lambda + (\lambda B^2/8)} \tag{22}$$

which allow for amplitude and phase determination. For the full nonlinear case, it is necessary to solve the set of Eqs. (15)–(18) numerically.

4. Stability of harmonic solutions

Stability analysis of the harmonic solutions is carried out by using the approximate Eqs. (9)–(12) with further assumptions

$$\frac{B^4}{48} \approx 0, \quad \frac{B^3}{16} \approx 0, \quad \frac{B^4}{12} \approx 0 \tag{23}$$

Determining derivatives $\dot{A}, \dot{\phi}_1, \dot{B}, \dot{\phi}_2$ from Eqs. (9)–(12) we get the so-called amplitude modulation equations, which can be written in shortened form

$$\dot{A} = f_1(A, \phi_1, B, \phi_2)$$
$$\dot{\phi}_1 = f_2(A, \phi_1, B, \phi_2)$$
$$\dot{B} = f_3(A, \phi_1, B, \phi_2)$$
$$\dot{\phi}_2 = f_4(A, \phi_1, B, \phi_2) \tag{24}$$

where

$$f_1 = \frac{W_{\dot{A}}}{W}, \quad f_2 = \frac{W_{\dot{\phi}_1}}{W}, \quad f_3 = \frac{W_{\dot{B}}}{W}, \quad f_4 = \frac{W_{\dot{\phi}_2}}{W} \tag{25}$$

Individual determinants in Eq. (25) are expressed as follows:

$$W = \begin{vmatrix} a_{11} & a_{12} & a_{13} & a_{14} \\ a_{21} & a_{22} & a_{23} & a_{24} \\ a_{31} & a_{32} & a_{33} & a_{34} \\ a_{41} & a_{42} & a_{43} & a_{44} \end{vmatrix}, \quad W_{\dot{A}} = \begin{vmatrix} a_0 & a_{12} & a_{13} & a_{14} \\ b_0 & a_{22} & a_{23} & a_{24} \\ c_0 & a_{32} & a_{33} & a_{34} \\ d_0 & a_{42} & a_{43} & a_{44} \end{vmatrix}$$

$$W_{\dot{B}} = \begin{vmatrix} a_{11} & a_0 & a_{13} & a_{14} \\ a_{21} & b_0 & a_{23} & a_{24} \\ a_{31} & c_0 & a_{33} & a_{34} \\ a_{41} & d_0 & a_{43} & a_{44} \end{vmatrix}, \quad W_{\dot{\phi}_1} = \begin{vmatrix} a_{11} & a_{12} & a_0 & a_{14} \\ a_{21} & a_{22} & b_0 & a_{24} \\ a_{31} & a_{32} & c_0 & a_{34} \\ a_{41} & a_{42} & d_0 & a_{44} \end{vmatrix}$$

$$W_{\dot{\phi}_2} = \begin{vmatrix} a_{11} & a_{12} & a_{13} & a_0 \\ a_{21} & a_{22} & a_{23} & b_0 \\ a_{31} & a_{32} & a_{33} & c_0 \\ a_{41} & a_{42} & a_{43} & d_0 \end{vmatrix} \tag{26}$$

The coefficients shown in determinants (26) are defined as

$$a_{11} = \alpha_1, \quad a_{12} = -2\vartheta A, \quad a_{13} = \mu\lambda\frac{\vartheta}{2}B\sin\Omega\left(\frac{B^2}{3} - 2\right), \quad a_{14} = -2\mu\lambda\frac{\vartheta}{2}B^2\cos\Omega \tag{27}$$

$$a_{21} = -2\vartheta, \quad a_{22} = -\alpha_1 A, \quad a_{23} = \mu\lambda\frac{\vartheta}{2}B\cos\Omega\left(\frac{B^2}{3} - 2\right), \quad a_{24} = 2\mu\lambda\frac{\vartheta}{2}B^2\sin\Omega \tag{28}$$

$$a_{31} = 0, \quad a_{32} = \lambda\vartheta AB\cos\Omega\left(\frac{B^2}{8} - 1\right), \quad a_{33} = \alpha_2, \quad a_{34} = -\vartheta B \tag{29}$$

$$a_{41} = 0, \quad a_{42} = \lambda\vartheta AB\sin\Omega\left(\frac{B^2}{8} - 1\right), \quad a_{43} = -\vartheta, \quad a_{44} = -\alpha_2 B \tag{30}$$

$$a_0 = q\cos\phi_1 - A + \vartheta^2 A - \frac{3}{4}\gamma A^3 + \mu\lambda B^2\left(\frac{\vartheta}{2}\right)^2\cos\Omega \tag{31}$$

$$b_0 = q\sin\phi_1 + \alpha_1\vartheta A - \mu\lambda B^2\left(\frac{\vartheta}{2}\right)^2\sin\Omega \tag{32}$$

$$c_0 = B\left(\frac{\vartheta}{2}\right)^2 - \lambda B + \frac{\lambda B^3}{8} + \frac{1}{2}\lambda\vartheta^2 AB\cos\Omega \tag{33}$$

$$d_0 = \alpha_2 B\frac{\vartheta}{2} + \frac{1}{2}\lambda\vartheta^2 AB\sin\Omega, \quad \text{where } \Omega = 2\phi_2 - \phi_1 \tag{34}$$

Perturbing the analysed solutions as follows, $A + \delta A$, $\phi_1 + \delta\phi_1$, $B + \delta B$, $\phi_2 + \delta\phi_2$, and then substituting them into Eq. (24), after which subtraction from the unperturbed solutions, and then taking into account the linear part of their power series expansions, we get a set of linear differential equations in the

variations δA, $\delta\phi_1$, δB, $\delta\phi_2$

$$\begin{bmatrix} \delta\dot{A} \\ \delta\dot{\phi}_1 \\ \delta\dot{B} \\ \delta\dot{\phi}_2 \end{bmatrix} = \mathbf{J} \begin{bmatrix} \delta A \\ \delta\phi_1 \\ \delta B \\ \delta\phi_2 \end{bmatrix}, \tag{35}$$

where the Jacobian $\mathbf{J}$ takes the form

$$\mathbf{J} = \begin{bmatrix} \frac{\partial f_1}{\partial A} & \frac{\partial f_1}{\partial \phi_1} & \frac{\partial f_1}{\partial B} & \frac{\partial f_1}{\partial \phi_2} \\ \frac{\partial f_2}{\partial A} & \frac{\partial f_2}{\partial \phi_1} & \frac{\partial f_2}{\partial B} & \frac{\partial f_2}{\partial \phi_2} \\ \frac{\partial f_3}{\partial A} & \frac{\partial f_3}{\partial \phi_1} & \frac{\partial f_3}{\partial B} & \frac{\partial f_3}{\partial \phi_2} \\ \frac{\partial f_4}{\partial A} & \frac{\partial f_4}{\partial \phi_1} & \frac{\partial f_4}{\partial B} & \frac{\partial f_4}{\partial \phi_2} \end{bmatrix}. \tag{36}$$

The stability of the approximate harmonic solutions depends on the eigenvalues of the Jacobian (36). If at least one of the roots has a positive real part then the solution becomes unstable.

5. Experimental setup

An experiment for the two degree-of-freedom model, presented schematically in Fig. 2, has been performed on an especially prepared experimental test stand. A photograph (Fig. 3) shows a real mechanical system in which the main parts are: the pendulum (1) which may achieve a full rotation, and the oscillator (2), together with additional masses (3). The mass moment of inertia of the pendulum can be modified by changing the masses (4) or the pendulum length. The pivot of the pendulum contains an optoelectronic converter MHK 40 (5) which has an angular measurement accuracy of $2\pi/2000$. Motion of the system is generated by an AC motor (7), an inverter (6) and a system which changes the rotation of the AC motor into translational motion. The damping coefficient of the linear viscous damper (8) is controlled by a hydraulic valve connected to an oil tank (9). The frequency of the vertical oscillations is controlled by the inverter. The amplitude of the kinematical excitation is set by the eccentric cam, fixed to the drive shaft. As an alternative option, a nonlinear

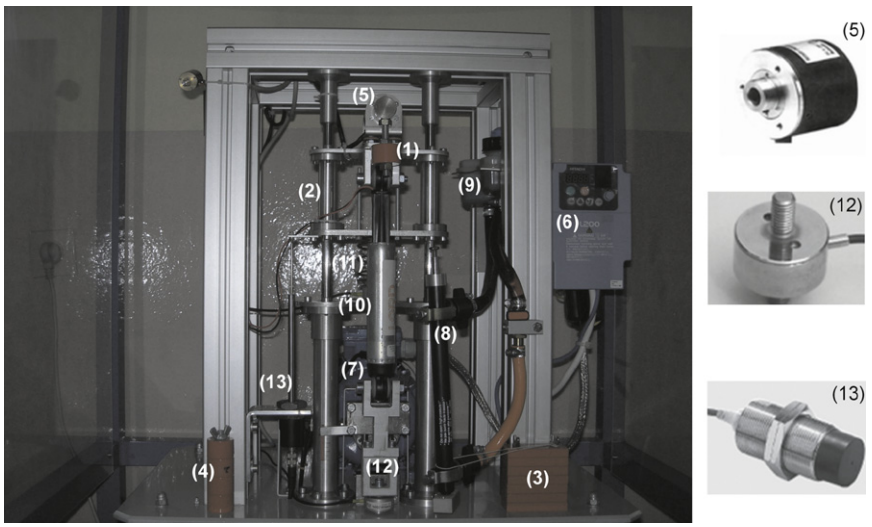

Fig. 3. General view of the experimental setup and its measurement devices.

composite magnetorheological damper RD 1097-01 (10) with a proper control system can be also applied. This MR damper has been effectively used to control the system motion to avoid unwanted situations—(see paper [13]).

The spring (11) which connects masses m_1 with the foundation is considered in the form of two variants, specifically linear or nonlinear, as required. Commercial software and hardware are used for data acquisition and control of the system. A strain gauge is fixed to the damper (12) to allow for damping force measurement. An additional strain gauge is mounted under the spring connecting the mass m_1 with the ground. The angle of rotation φ of the pendulum and the displacement x of the oscillator are measured by an optoelectronic converter and the special proximity detector (13). Velocity and acceleration of the pendulum and oscillator are calculated from received signals by their numerical derivation. Application of additional sensors allows also for measuring the damping force and the force transmitted on the foundation.

6. Numerical results and experimental verification

Numerical analysis of the system is carried out on the basis of data taken from a practical system as shown in Fig. 3. Dimensionless parameters, calculated according to Eq. (6) take these values,

$$\alpha_1 = 0.261354, \quad \alpha_2 = 0.1, \quad q = 2.45094, \quad \mu = 17.2278, \quad \lambda = 0.127213, \quad \gamma = 0. \tag{37}$$

Direct numerical simulations have been performed on the basis of Eqs. (4) and (5) in Matlab–Simulink and the Dynamics package [14] by using the fourth-order Runge–Kutta method. Initial conditions are fixed as: $x = 0$, $x' = 0$, $\varphi = 0.1$, $\varphi' = 0$. Analytical results have been presented for the same data by using equations derived by the HBM as presented in Section 4.

In this type of autoparametric system with an attached pendulum, near the frequency $\vartheta = 1$, there exists a region where, due to internal excitation, the principal parametric resonance takes place. The resonance curves of the pendulum and the oscillator are presented in Fig. 4. This resonance is manifested by relatively small vibrations of the oscillator with frequency ϑ and oscillations of the pendulum with frequency $\vartheta/2$. The solid line and black dots in Fig. 4 denote stable amplitudes (trivial and nontrivial) obtained by analytical and experimental investigations, the dashed line and white points represent unstable results, respectively. The stability of the system has been determined analytically from the eigenvalues of the Jacobian matrix (36).

Inside the resonance the motion of the oscillator is reduced by the pendulum oscillations, which play the role of a dynamical absorber. Outside this region this phenomenon fades out and then the oscillator's amplitudes tend to high values (see dashed line in Fig. 4b).

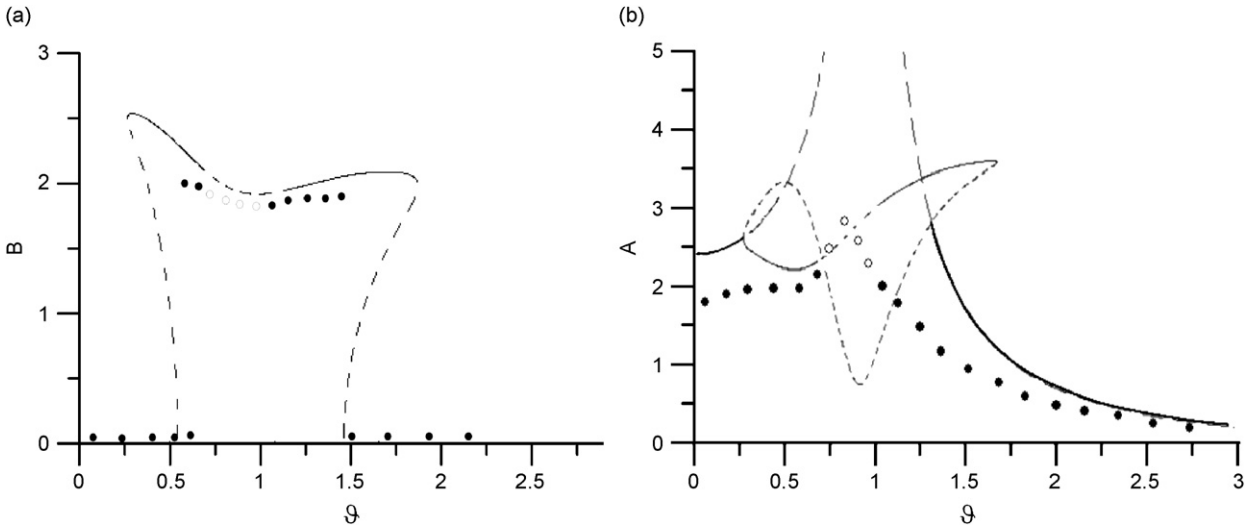

Fig. 4. Analytical resonance curve and experimental results of the oscillator (a) and the pendulum (b), $\alpha_1 = 0.261354$, $\alpha_2 = 0.1$.

As can be seen in Fig. 4, there exists an unstable region in the middle of the resonance, located around the amplitude 'well'. If the system works in this area, then regular motion becomes quasi-periodic or chaotic [12]. Transition to this region can lead to unexpected increase of amplitude and eventually to destruction of the system. Therefore, it is very important to avoid such situations. If the system has to work in this region, then we should know how to reduce or control the system dynamics.

Fig. 5 presents a numerical bifurcation diagram and the corresponding Lyapunov exponents (Fig. 5b), near the main parametric resonance. If the frequency of excitation ϑ takes a value from the range ~0.6 to 0.62, then chaotic motions appear. It is interesting that this motion is represented by an irregular attractor which consists only of swings ('chaotic swings'). For the frequency ϑ~0.63–0.72 and ϑ~0.98–1.19, chaotic motions are composed of both rotation and swinging of the pendulum. If the frequency of excitation is located between 0.73 and 0.97 then the pendulum performs full rotations. Experimental tests confirm unstable regions existence in which the pendulum executes chaotic motions (rotation and swinging) or full rotations. However, chaotic motions consisting only of swinging have not been detected experimentally. This could probably be caused by dynamically changed damping in the pendulum pivot and in the oscillator. This could eliminate the very narrow region of chaotic swings, discovered numerically.

In Fig. 6a and b, experimental time histories showing transition to the chaotic motion and rotation of the pendulum are presented. They are in accordance with the Lyapunov exponent diagram obtained numerically from the model.

The chaotic attractor, corresponding to the time history in Fig. 6a for $\vartheta = 0.7$, is presented in Fig. 7. Fig. 7a shows the numerical attractor for the pendulum. To confirm this result by an experimental test, the attractor from a real signal is reconstructed (Fig. 7b). For the phase portrait reconstruction only one signal of the angular velocity of the pendulum is used [15]. This choice of signal makes the analysis easier because in the velocity domain the rotation of the pendulum is eliminated.

The attractor reconstruction is carried out using a time series analysis application [15]. This software for time series analysis is based on the theory of nonlinear deterministic dynamical systems. In order to undertake attractor reconstruction, the time delay (τ_1) is calculated using the mutual information method, providing important information about reasonable delay times, while the false neighbours statistic is applied for estimating the embedding dimension. An exact mathematical description of these functions is given in Refs. [16,17]. The result of the analysis is presented in Fig. 7b. Both the numerical and experimental attractors have similar shape, arrangement, and dimension. This analysis fully confirms agreement of theoretical and experimental investigations.

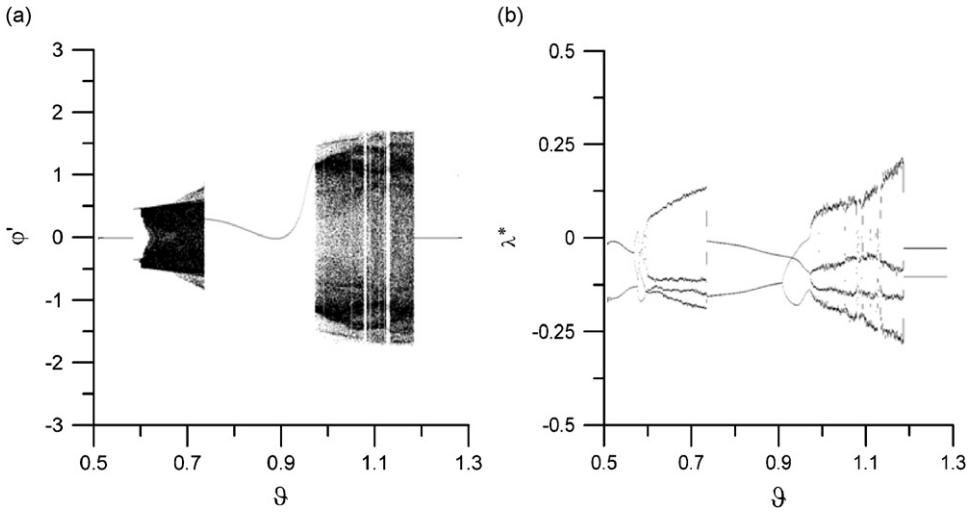

Fig. 5. Bifurcation diagram (a) and Lyapunov exponents (b), $\alpha_1 = 0.261354$, $\alpha_2 = 0.1$.

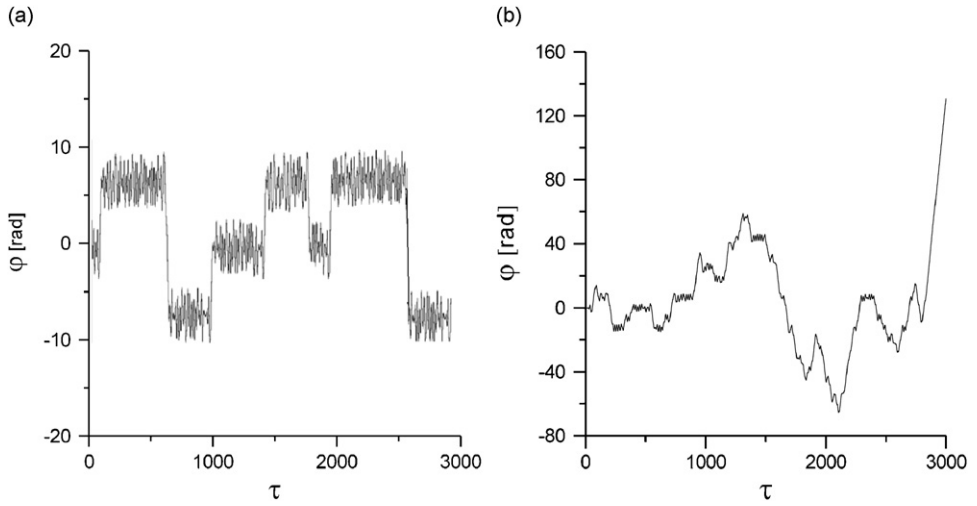

Fig. 6. Experimental time histories of the pendulum, (a) chaotic motions for $\vartheta = 0.7$ and (b) transition to rotation for $\vartheta = 0.73$.

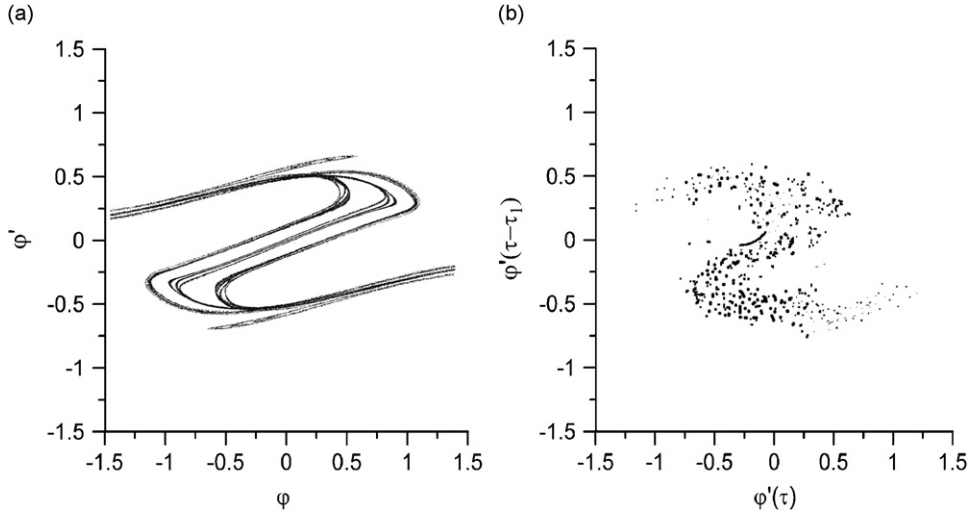

Fig. 7. Chaotic numerical attractor (a) and reconstructed experimental attractor (b), for frequency $\vartheta = 0.7$.

7. Influence of the system parameters on the instability region

Considering that the pendulum is designed as a dynamical vibration absorber (Fig. 1), it is necessary to recognise the reason of the occurrence of the instability region and to find the system parameters' influence on this phenomenon. The set of parameters should be chosen carefully, to eliminate the instability, but not to reduce the range of active pendulum operation. The first possible intuitive solution is to increase the system damping.

Figs. 8 and 9 present the influence of damping on the pendulum amplitudes. Both graphs are plotted on the basis of Eq. (21). From the results of Fig. 8, we can reduce the instability area by increasing the damping of the oscillator α_1. The critical value of those damping coefficients $\alpha_1 \approx 0.6$ causes total vanishing of the region. The influence of this parameter is clearly visible on the surface cross-sections in Fig. 8b. The disadvantage of such a solution is that the right hand side of the resonance curve (the higher frequency side) is totally reduced.

The increase of the pendulum damping in the pivot causes reduction both to the right and the left hand sides of the resonance curves, which essentially decreases the effectiveness of the pendulum as a dynamical damper

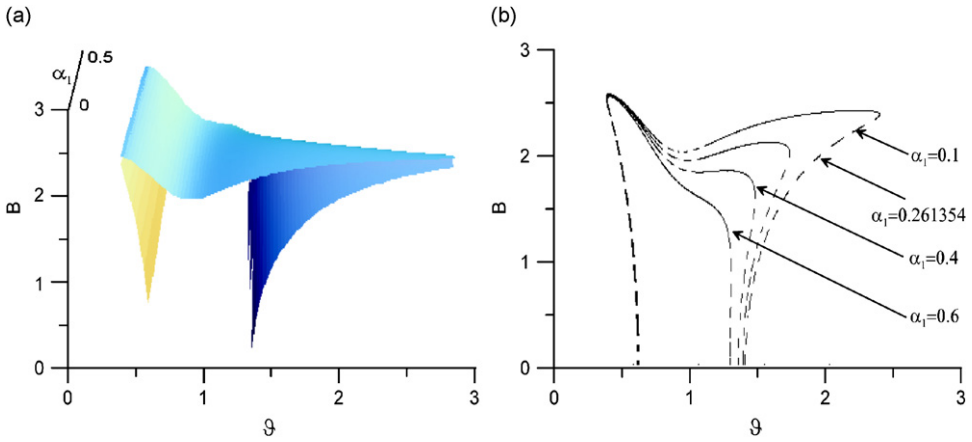

Fig. 8. Pendulum's amplitude versus excitation frequency and damping, 3D graph (a) and cross-sections for different coefficients of oscillator damping α_1 (b).

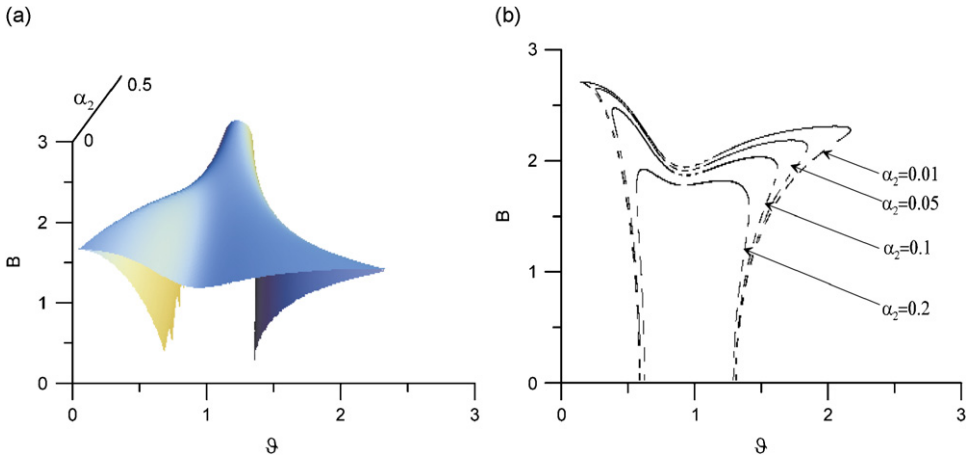

Fig. 9. Pendulum's amplitude versus excitation frequency and damping, 3D graph (a) and cross-sections for different coefficients of the pendulum damping α_2 (b).

(Fig. 9). For damping in the pivot of $\alpha_2 \approx 0.5$, this instability does not exist at all, however a very narrow region of absorption is the price we pay for this solution.

Fig. 10 presents the influence on the excitation amplitude q on the unstable region. If the value of excitation amplitude is increasing then the instability effect is still present, and the area is widened and the pendulum oscillations increase dangerously.

The dynamics of the system strongly depend on the values of the nonlinear terms which couple the main structure (the oscillator) and the pendulum. The response of the system is very sensitive to changes to the parameters λ and μ. Parameter λ couples the oscillator and pendulum motion (Eqs. (4) and (5)). Parameter μ only appears in the oscillator equation of motion and plays the role of a gain in the product $\mu\lambda$ in the oscillator equation. In a real system, the length of the pendulum and its mass moment of inertia are responsible for these parameters values.

The influence of both parameters λ and μ on the pendulum oscillation around the principal parametric resonance is presented in Figs. 11 and 12, respectively. These plots allow one to determine a proper selection of the pendulum parameters, required for a given structure (the oscillator). However, modification of the parameter λ or μ while the system vibrates in order to control the response online could be rather difficult.

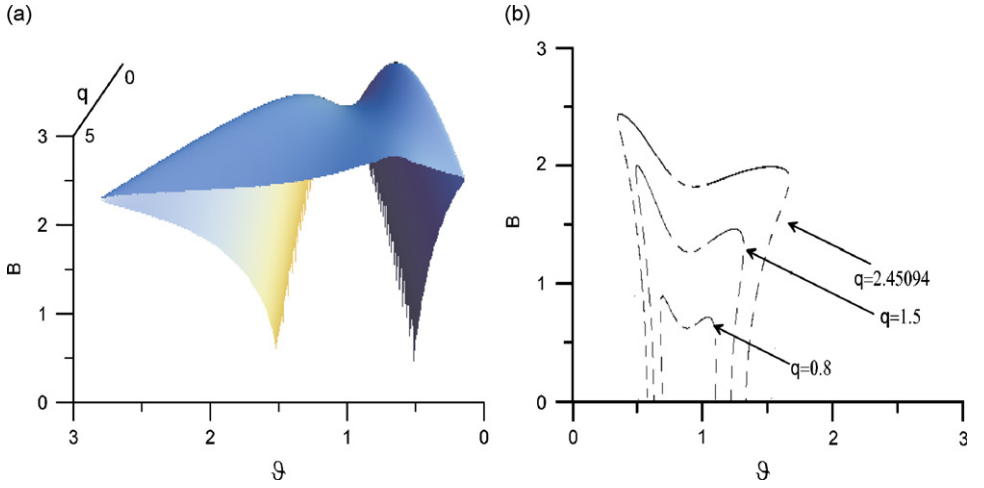

Fig. 10. Pendulum's amplitude versus excitation frequency and excitation amplitude, 3D graph (a) and cross-sections for different amplitudes of excitation q (b).

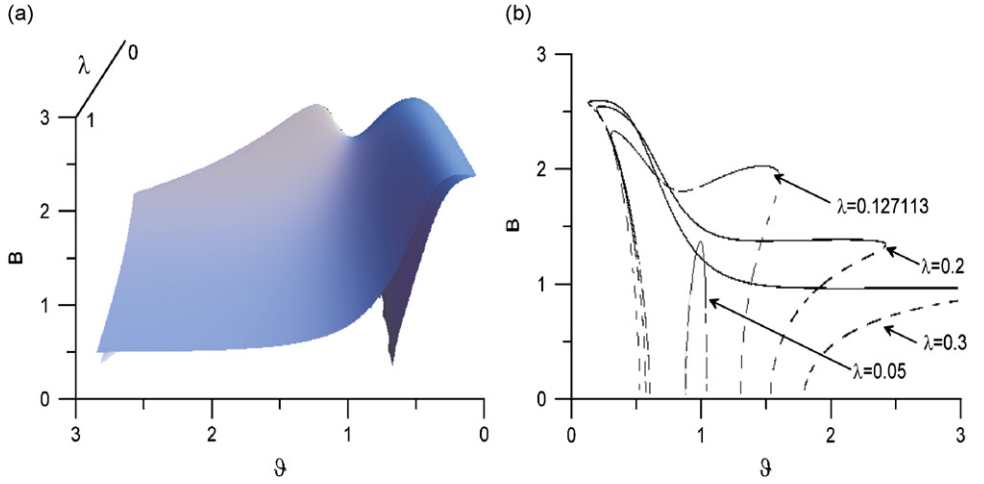

Fig. 11. Pendulum's amplitude versus excitation frequency and parameter λ, 3D graph (a) and cross-sections for different coefficients λ (b).

Another proposal to change the system dynamics is to include the nonlinear stiffness of the supported spring (Eq. (1)). Because it has not been possible to solve this nonlinear case analytically, the influence of the supporting spring stiffness is analysed by numerical methods.

Figs. 13 and 14 show bifurcation diagrams for different parameters γ. For a very small nonlinearity of $\gamma = 0.01$, we observe two chaotic regions where, if γ increases, up to $\gamma = 0.02$, then the first chaotic region is reduced and moved, together with the second area, to the right side. This result can be explained by the stiffening effect. Moreover, the working area of the pendulum regular swinging is wider.

The bifurcation diagrams calculated for larger values of the γ parameter, $\gamma = 0.05$ and 0.1, are shown in Fig. 14. For $\gamma = 0.05$ chaos disappears which means that in the range $\vartheta \sim 0.5$–2 the instable region is completely eliminated. Further increase of stiffness lead to a new chaotic region arising (Fig. 14b), but the subharmonic pendulum response is very wide.

Exemplary numerical chaotic attractors are given in the Poincaré section in Fig. 15. In both examples, the chaotic attractor consists of full rotation and swinging of the pendulum.

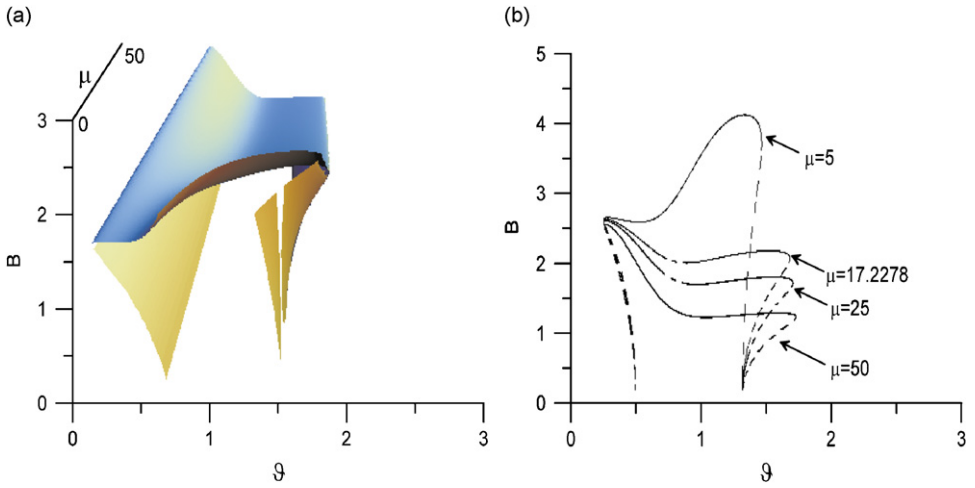

Fig. 12. Pendulum's amplitude versus excitation frequency and parameter μ, 3D graph (a) and cross-sections for different coefficients μ (b).

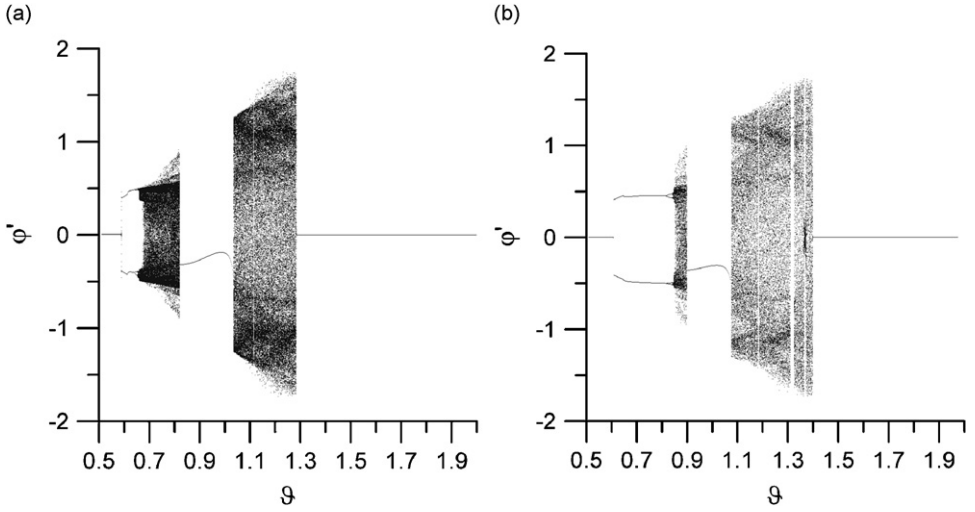

Fig. 13. Bifurcation diagram of the pendulum for $\gamma = 0.01$ (a) and $\gamma = 0.02$ (b).

Introduction of stiffness nonlinearity seems to be a promising method for improving the dynamical absorption phenomenon. Nevertheless, bearing in mind that for different initial conditions the nonlinearity may lead to several steady states, the basins of attraction of the solution have also to be checked. In Fig. 16, for the frequency $\vartheta = 0.65$, $\gamma = 0.01$, we observe two possible solutions, represented by attractors Nos. 1 and 2. If the stiffness rises, up to $\gamma = 0.02$ (Fig. 17), then there are three solutions with relevant basins of attraction: Nos. 1 and 2 denote the two double-point attractors, and No. 3—the six-point attractor.

Fig. 18a and b presents numerical time histories for $\gamma = 0.02$ and frequency $\vartheta = 0.65$ for two different initial conditions of the pendulum, corresponding to the subharmonic response with the 1:2 and 1:6 periods ratio.

It is worth pointing out another interesting phenomenon which may appear if the system works in the unstable region. Assuming again $\gamma = 0$, we can notice for $\vartheta = 0.59$, the pendulum's vibration centre is shifted. Depending on the initial conditions the centre of the angle φ may be shifted in the positive (Fig. 19b) or the negative (Fig. 19a) direction. The two possible shifts are symmetric around the lower static position of the pendulum. The shift of the pendulum's vibration has been detected in the real setup, too. An experimental time history of the pendulum is presented in Fig. 20a and a relevant phase trajectory in Fig. 20b.

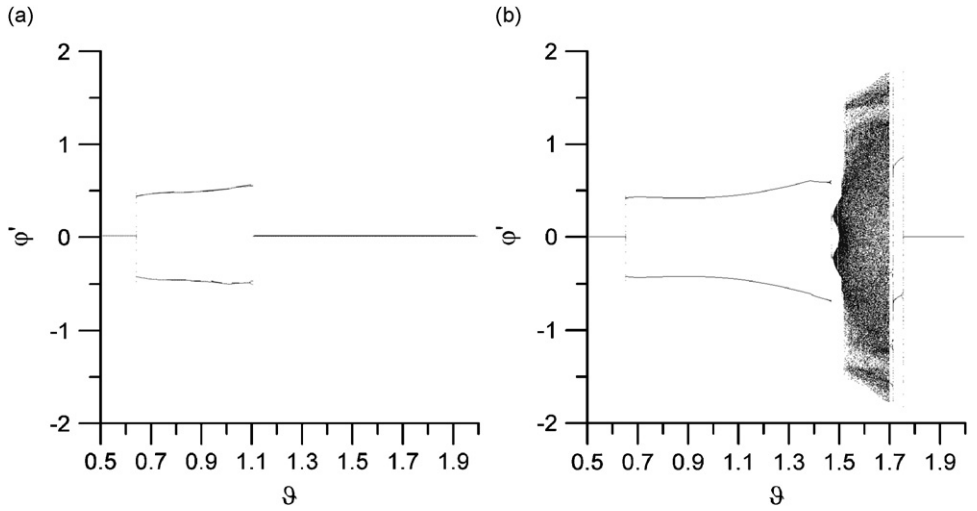

Fig. 14. Bifurcation diagram of the pendulum for $\gamma = 0.05$ (a) and $\gamma = 0.1$ (b).

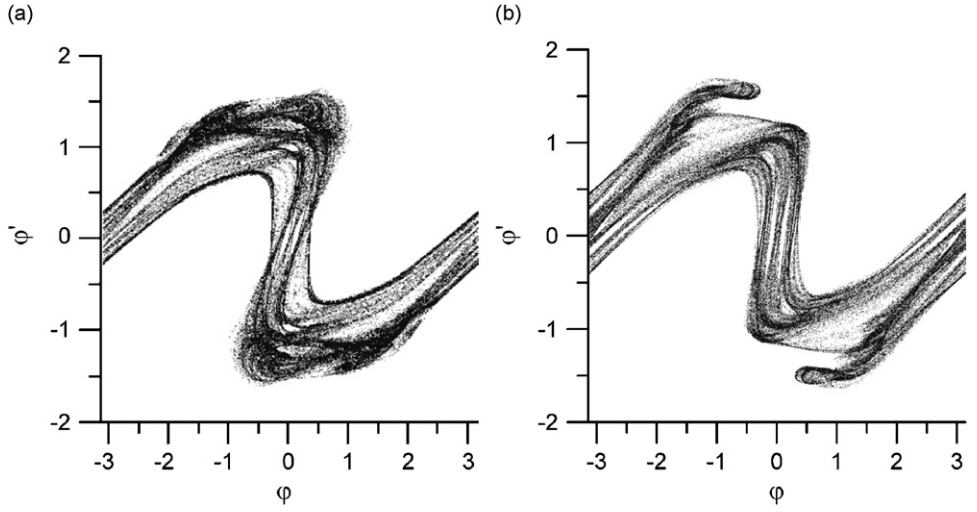

Fig. 15. Poincaré maps for the pendulum, $\gamma = 0.02$, $\vartheta = 1.25$ (a), and $\gamma = 0.1$, $\vartheta = 1.6$ (b).

In experimental tests only the positive centre shift has been found. It probably results from a difference between real and modelled basins of attraction.

8. Conclusions

The autoparametric system considered in this paper exhibits an instability region near the principal parametric resonance for some sets of parameters. This phenomenon may lead to a rotation of the pendulum, or to its chaotic motion, composed of both swinging and rotation. Existence of this instability is not required if the pendulum is to be designed as a dynamical absorber. The unpredictable increase of the vibrations may eventually destroy the protected structure. An increase in damping of the pendulum causes decaying of the instability but also a big reduction of the resonant curve, an unwanted effect from the vibration dynamical absorption point of view. Unwanted motion can also be eliminated by proper choice of the pendulum parameters, but these parameters cannot be modified online, as the pendulum operates. Another solution for improving the system's behaviour is to introduce a nonlinear supporting

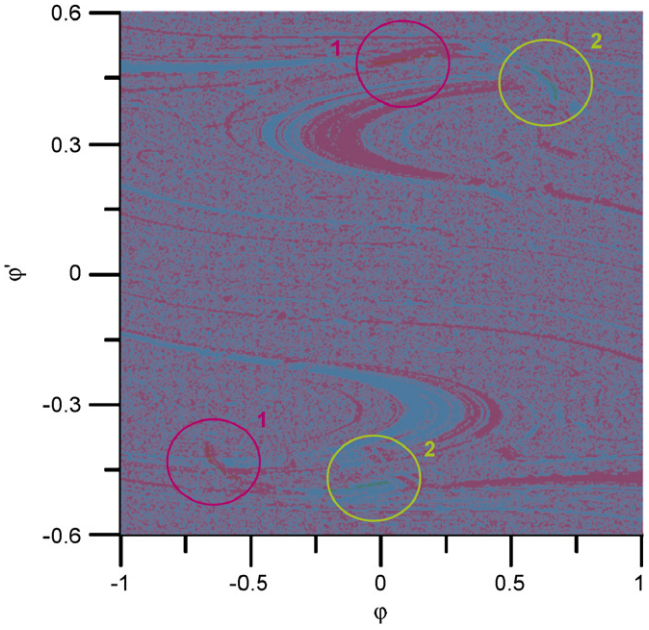

Fig. 16. Basins of attraction of the pendulum, $\vartheta = 0.65$, $\gamma = 0.01$.

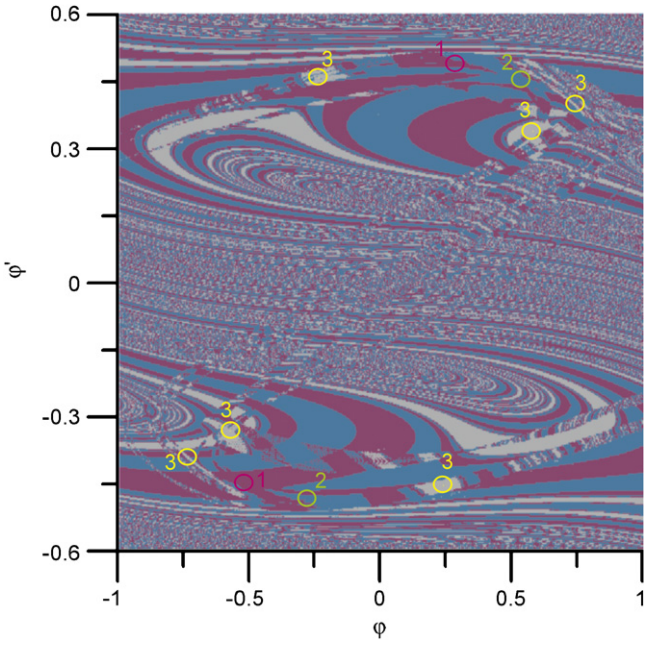

Fig. 17. Basins of attraction of the pendulum, $\vartheta = 0.65$, $\gamma = 0.02$.

spring, which rejects or shifts the chaotic response and widens the range of the effective absorption interval. However, the additional nonlinearity introduces new attractors with their basins of attractions. Therefore, the proposed new design can be combined with a modification of the oscillator damping, which also reduces the instability region. A promising device which can be applied in the system is a magnetorheological damper together with a smart spring which could allow for online control of the system motion.

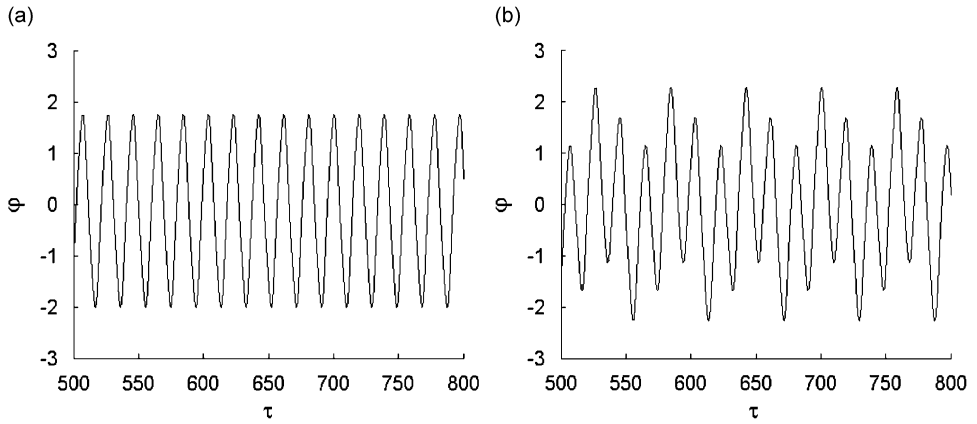

Fig. 18. Numerical time histories of the pendulum for stiffness coefficient $\gamma = 0.02$, $\vartheta = 0.65$, and for different initial conditions of the pendulum, $\varphi = 0.1$ (a) and $\varphi = 0.7$ (b).

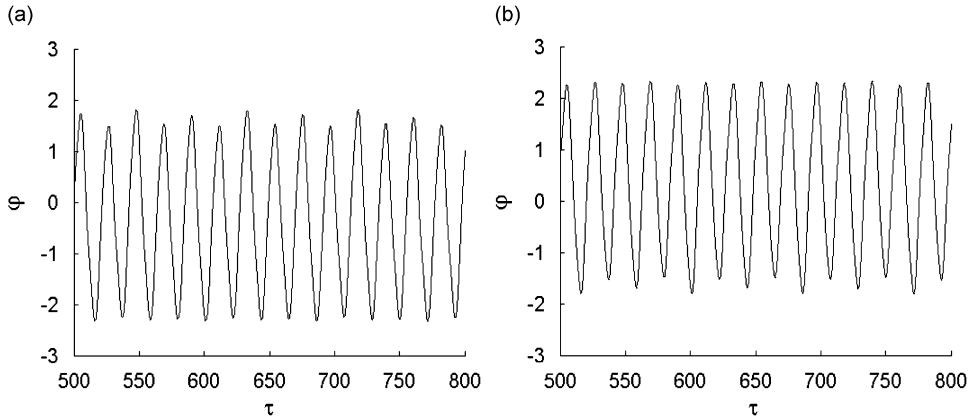

Fig. 19. Numerical time histories of the pendulum for linear system ($\gamma = 0$) and $\vartheta = 0.59$, and different initial conditions of the pendulum $\varphi = 0.1$ (a) and $\varphi = 0.5$ (b).

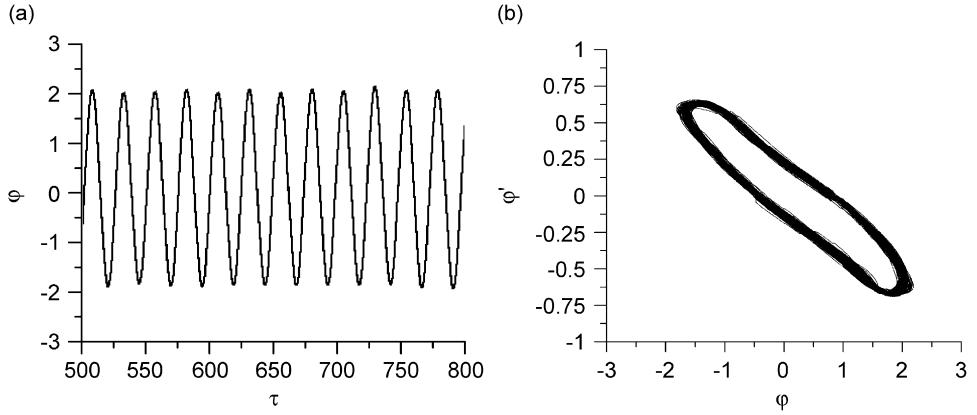

Fig. 20. Experimental time histories of the pendulum for linear system (a) and phase portrait (b) for initial condition of the pendulum $\varphi = 0.1$, and $\vartheta = 0.59$, $\gamma = 0$.

Numerical and analytical results for regular and chaotic vibrations are in good accordance with experimental tests. The attractor, reconstructed on the basis of real signals, confirms the possible chaotic behaviour of the system. The experimental investigations of the real design with the nonlinear spring and the magnetorheological damper will be carried out in future work.

Acknowledgements

The work is supported by Grants nos. N502 049 31/1449 and 65/6.PR UE/2005/7 from the Polish Ministry of Science and Higher Education.

References

[1] M.P. Cartmell, J. Lawson, Performance enhancement of an autoparametric vibration absorber by means of computers control, *Journal of Sound and Vibration* 2 (1994) 173–195.
[2] B.F. Spencer, M.K. Sain, Controlling buildings: a new frontier in feedback, *Special issue of the IEEE Control Systems Magazine on Emerging Technology* 17 (6) (1997) 19–35.
[3] A. Natthapong, W. Pennung, Vibration suppression of a 90 m tall steel stack by using a high-damping tuned mass damper, *The Eighth East Asia-Pacific Conference on Structural Engineering and Construction*, Nanyang Technological University, Singapore, 5–7 December 2001, Paper no. 1316.
[4] A. Tondl, T. Ruijgork, F. Verhulst, R. Nabergoj, *Autoparametric Resonance in Mechanical System*, Cambridge University Press, New York, 2000.
[5] K. Kecik, J. Warminski, K. Szabelski, Drgania regularne i chaotyczne układu mechanicznego z wahadłem, Materiały Konferencyjne, I Kongres Mechaniki Polskiej, Warszawa, 28–31 Sierpnia 2007 (in Polish).
[6] B. Banerjee, A.K. Bajaj, P. Davies, Resonant dynamics of an autoparametric system: a study using higher-order averaging, *International Journal of Non-linear Mechanics* 31 (1996) 21–39.
[7] H. Hatwal, A.K. Mallik, A. Ghosh, Forced nonlinear oscillations of an autoparametric system. Part 1. Periodic responses, *Journal of Applied Mechanics, Transactions of the American Society of Mechanical Engineers* 50 (1983) 657–662.
[8] H. Hatwal, A.K. Mallik, A. Ghosh, Forced nonlinear oscillations of an autoparametric system. Part 2. Chaotic responses, *Journal of Applied Mechanics, Transactions of the American Society of Mechanical Engineers* 50 (1983) 663–668.
[9] H. Hatwal, A.K. Mallik, A. Ghosh, Non-linear vibrations of a harmonically excited autoparametric system, *Journal of Sound and Vibration* 81 (1982) 153–164.
[10] K. Bajaj, S.I. Chang, J.M. Johnson, Amplitude modulated dynamics of a resonantly excited autoparametric two degree-of-freedom system, *Nonlinear Dynamics* 5 (1994) 433–457.
[11] J. Warminski, K. Kecik, Autoparametric vibration of a nonlinear system with pendulum, *Mathematical Problems in Engineering* (2005), Article ID 80705.
[12] Y. Song, H. Sato, Y. Iwata, T. Komatsuzaki, The response of a dynamic vibration absorber system with a parametrically excited pendulum, *Journal of Sound and Vibration* 259 (2003) 747–759.
[13] J. Warminski, K. Kecik, Control of regular and chaotic motions in autoparametric system with pendulum, in: J. Awrejcewicz (Ed.), Modeling, Simulation and Control of Nonlinear Engineering Dynamical Systems, Special issue of Springer, 2008, in press.
[14] H.E. Nusse, J.A. Yorke, *Dynamics: Numerical Explorations*, Springer, New York, 1994.
[15] H.D.I. Abarbanel, *Analysis of Observed Chaotic Data*, Springer, New York, 1996.
[16] H. Kantz, T. Schreiber, *Nonlinear Time Series Analysis*, Cambridge University Press, 1999.
[17] R. Hegger, H. Kantz, Practical implementation of nonlinear time series methods: the TISEAN package, *Chaos* 9 (1999) 413–435.